Ductility inverse-mapping method for SDOF systems including passive dampers for varying input level of ground motion

Hyeong-Gook Kim, Shinta Yoshitomi, Masaaki Tsuji and Izuru Takewaki*

*Department of Architecture & Architectural Engineering, Kyoto University,
Kyotodaigaku-katsura, Kyoto 615-8540, Japan*

Abstract.   A ductility inverse-mapping method for SDOF systems including passive dampers is proposed which enables one to find the maximum acceleration of ground motion for the prescribed maximum response deformation. In the conventional capacity spectrum method, the maximum response deformation is computed through iterative procedures for the prescribed maximum acceleration of ground motion. This is because the equivalent linear model for response evaluation is described in terms of unknown maximum deformation. While successive calculations are needed, no numerically unstable iterative procedure is required in the proposed method. This ductility inverse-mapping method is applied to an SDOF model of bilinear hysteresis. The SDOF models without and with passive dampers (viscous, visco-elastic and hysteretic dampers) are taken into account to investigate the effectiveness of passive dampers for seismic retrofitting of building structures. Since the maximum response deformation is the principal parameter and specified sequentially, the proposed ductility inverse-mapping method is suitable for the implementation of the performance-based design.

Keywords: capacity spectrum method; maximum ground acceleration; response spectrum; passive dampers; ductility inverse-mapping method; demand and capacity spectra; equivalent linear model; performance-based design

1. Introduction

The capacity spectrum method (ATC 1996, BSSC 1997, Freeman 1975, 1998, Fajfar 1999) is used in many seismic design codes all over the world. This design method adopts the demand spectrum and the capacity spectrum as the load effect and the corresponding structural resistance, respectively. Recently some extensions have been made in the inclusion of higher-mode effects or the development of non-iterative procedures (Chopra *et al* 2004, Lin and Miranda 2004, Kalkan and Kunnath 2006, Guyader and Iwan 2006, Gencturk and Elnashai 2008). However, there remain some difficulties in the avoidance of non-convergence or multiple solution problems and in the construction of empirical formulas for equivalent linear models. Especially the empirical formulas (for example Lin and Miranda 2004) for equivalent linear models have to be constructed for each hysteretic restoring-force characteristic and this procedure may be cumbersome and closely related

to the accuracy of the method.

A ductility inverse-mapping method is proposed in this paper which enables structural designers to find the maximum acceleration of ground motion for the prescribed maximum response deformation. In the conventional capacity spectrum method, the maximum inelastic response deformation is computed through iterative procedures for the prescribed maximum acceleration of ground motion. This is because the equivalent linear model (equivalent stiffness and viscous damping coefficient) is described in terms of unknown maximum inelastic deformation (or ductility ratio). While successive calculations are needed, no numerically unstable iterative procedure is required in the proposed ductility inverse-mapping method. Furthermore, the successive construction of the relation of the maximum acceleration of ground motion with the maximum response deformation makes it possible to know directly and simultaneously the response deformations to several desired or interested input levels of ground motion. As a similar pioneering approach, Hayashi (2002) and Hayashi *et al*. (2008) proposed another inverse method (Equivalent performance response spectra) to find the equivalent spectral acceleration for a specified maximum deformation. In contrast to the present work, their method is aimed at finding the response spectral acceleration, not the maximum value of ground motions (acceleration or velocity), for the specified deformation. It is shown here that the best or better equivalent damping ratio of passively controlled structures can be derived by changing the prescribed deformation levels gradually.

This ductility inverse-mapping method is applied to an SDOF model of bilinear hysteresis. The SDOF models without and with passive dampers (viscous, visco-elastic and hysteretic dampers) are taken into account to investigate the effectiveness of passive dampers for seismic retrofitting of various types of buildings. It is shown that, since the maximum response deformation is the principal parameter and specified sequentially, the proposed ductility inverse-mapping method is suitable for the implementation of the performance-based design. The concept of effective deformation ratio is also proposed to enhance the reliability and accuracy of prediction of inelastic dynamic responses.

2. Conventional capacity spectrum method

The capacity spectrum method was originally developed by Freeman (1975) and its applicability to practical seismic design was discussed during and after 1990's (for example, ATC 1996, BSSC 1997, Freeman 1975, 1998, Fajfar 1999, Chopra *et al*. 2004, Kalkan and Kunnath 2006, Gencturk and Elnashai 2008). The merit of the capacity spectrum method comes from its simplicity. The demand spectrum is usually described by the equivalent linear model in terms of the inelastic response spectrum method. On the other hand, the capacity spectrum is usually derived by the static pushover analysis. In the usual capacity spectrum method, the maximum inelastic deformation of a structure is estimated iteratively. This iteration consists of (i) the assumption of the response deformation (ductility), (ii) the construction of an equivalent linear model (usually secant stiffness and equivalent viscous damping ratio), (iii) the estimation of the deformation in terms of the equivalent linear model and (iv) the convergence check of the correspondence of the demand (corresponding to assumed equivalent natural period and damping ratio) and capacity spectra. The outline of the conventional capacity spectrum method is shown in Fig. 1.
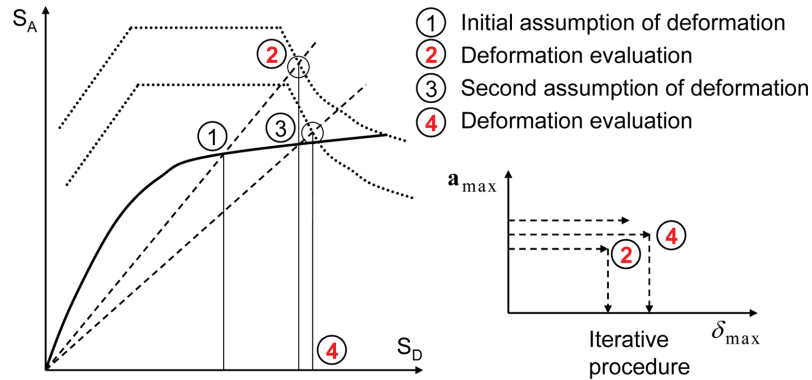
Fig. 1 Outline of conventional capacity spectrum method

3. Concept of ductility inverse-mapping method

In the conventional capacity spectrum method, the input level (for example the maximum acceleration) of ground motion is prescribed. Then the maximum inelastic deformation is inevitably derived iteratively because the parameters of equivalent linear models are functions of unknown maximum inelastic deformation. In this case, there exist some difficulties of non-convergence or multiple solution problems. While some successful attempts have been done (for example Hayashi 2002, Lin and Miranda 2004) for non-iterative procedures, the empirical formulas for equivalent linear models have to be constructed for each hysteretic restoring-force characteristic. The construction of these empirical formulas may be cumbersome and the validity of these empirical formulas certainly affects the accuracy of such methods.

To overcome these difficulties, a ductility inverse-mapping method is proposed here. The conceptual diagram and flowchart of the proposed ductility inverse-mapping method are shown in Fig. 2. In the proposed ductility inverse-mapping method, the maximum inelastic deformation is given successively from rather smaller values (Step 1-1 in Fig. 2) and the corresponding input level of ground motion is determined (Step 1-2 in Fig. 2) by using the relation between the input level of ground motion and the inelastic deformation. This procedure is an inverse procedure to the process taken in the conventional capacity spectrum method. For successive specification of maximum deformation, one can obtain the spectral acceleration (Step 1-3 in Fig. 2). Once the relation between the input level of ground motion and the maximum inelastic deformation is derived (Step 1-2 and 2-2 in Fig. 2), the structural designers can find the maximum inelastic deformation (Step 2-2 in Fig. 2) and spectral acceleration (Step 2-3 in Fig. 2) which the structure exhibits to the specified input level (specified at Step 2-1 in Fig. 2) of ground motion. It may be appropriate to call the proposed ductility inverse-mapping method as a dynamic pushover analysis method.

Although a method of equivalent linearization is used in the present paper, other methods can be used if desired. There is no difficulty in this point. The necessity of iteration does not depend on what kind of methods of equivalent linearization is used. The necessary condition is that the equivalent stiffness and damping are described in terms of the maximum inelastic deformation (or ductility). The effective natural period which can be obtained from the secant stiffness for the specified maximum deformation can also be included in the model of equivalent linearization (for example Guyader and Iwan 2006). The key point is concerned with the fact that the maximum
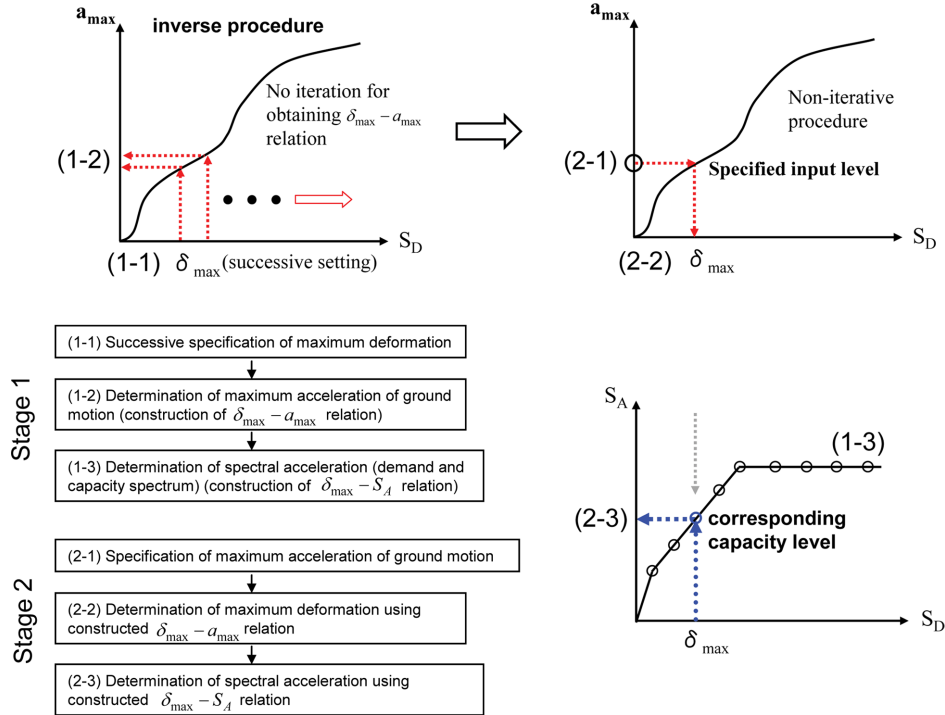
Fig. 2 Conceptual diagram and flowchart of proposed ductility inverse-mapping method

inelastic deformation is specified in the proposed ductility inverse-mapping method.

It should be noted that Hayashi (2002) and Hayashi *et al*. (2008) developed almost the same transformation procedure from the prescribed deformation to the response acceleration spectrum (Equivalent performance response spectra). Their method is an original one to avoid iteration for variable input levels. In contrast to the present work, their method concentrates primarily on the response acceleration, not the input level (ground acceleration or velocity), for the specified deformation.

4. Numerical examples

The objective of the ductility inverse-mapping method is to provide structural designers or engineers with preferable passive damper systems for retrofitting of various-type houses or buildings (see Fig. 3). Furthermore the objective of this paper is not to compare the accuracy of both methods (capacity spectrum method and ductility inverse-mapping method) because the merit of the proposed ductility inverse-mapping method is to be able to obtain a series of solutions corresponding to a series of input levels. When the input ground motion level in the ductility inverse-mapping method coincides with that of the capacity spectrum method, the results of both methods coincide because '*the governing equations of both methods are the same*'. However the accuracy of the capacity spectrum method depends on the initial estimate of the deformation ductility factor and the number of iterations employed. The iteration in the ductility inverse-mapping method is unnecessary because the target maximum inelastic deformation (the key parameter for the
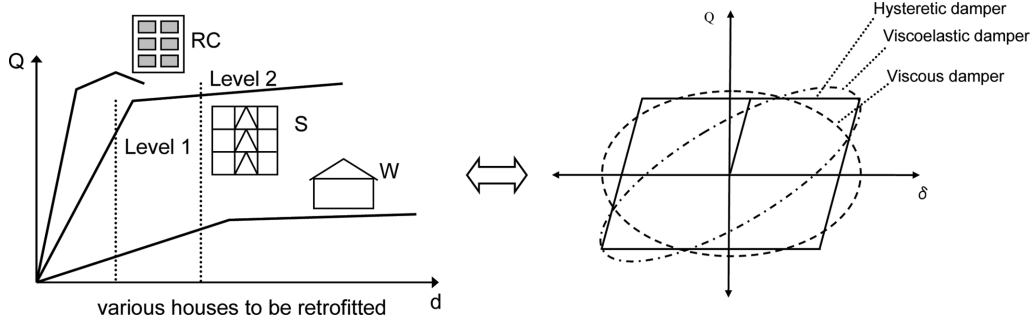
Fig. 3 Effective passive damper systems for retrofitting of various-type houses or buildings

construction of the equivalent linear model) is given in the ductility inverse-mapping method. It should also be reminded that the input ground motion level is not specified in the proposed ductility inverse-mapping method and it is derived directly. This is the reason why the proposed ductility inverse-mapping method does not need iteration at all. The proposed method is not a simplified version of capacity spectrum method, but the exact one for the same input ground motion level as specified in the capacity spectrum method.

In this section two structural models are considered. One is an elastic frame and the other is an inelastic frame (steel, reinforced concrete and wood structures).

4.1 Design response spectrum by Newmark and Hall (1982)

The design response spectrum-compatible ground motions can be used as the representative input motions. A simplified version of the design displacement response spectrum by Newmark and Hall (1982) can be expressed in terms of undamped natural circular frequency ω and damping ratio h by

$$S_D(\omega;h) = S_D^A(\omega;h) = \frac{\ddot{u}_{g\max}\{3.21 - 0.68\ln(100h)\}}{\omega^2} = \frac{\ddot{u}_{g\max}A_A(h)}{\omega^2} \quad (\omega_U \leq \omega) \tag{1a}$$

$$S_D(\omega;h) = S_D^V(\omega;h) = \frac{\dot{u}_{g\max}\{2.31 - 0.41\ln(100h)\}}{\omega} = \frac{\dot{u}_{g\max}A_V(h)}{\omega} \quad (\omega_L \leq \omega \leq \omega_U) \tag{1b}$$

$$S_D(\omega;h) = S_D^D(\omega;h) = u_{g\max}\{1.82 - 0.27\ln(100h)\} = u_{g\max}A_D(h) \quad (\omega \leq \omega_L) \tag{1c}$$

In Eqs. 1(a)-(c), $u_{g\max}$, $\dot{u}_{g\max}$ and $\ddot{u}_{g\max}$ are the maximum ground displacement, velocity and acceleration, respectively, and $A_A(h)$, $A_V(h)$ and $A_D(h)$ are the acceleration, velocity and displacement amplification factors, respectively. The circular frequencies ω_U and ω_L in Eqs. 1(a)-(c) are derived from the relations $S_D^A(\omega_U;h) = S_D^V(\omega_U;h)$, $S_D^V(\omega_L;h) = S_D^D(\omega_L;h)$.

4.2 Equivalent linear model

The building structure is modeled into an SDOF model. At first the building structure modeled as an SDOF model and the hysteretic damper are assumed to obey normal bilinear (elastic-perfectly plastic) hysteretic rules. The equivalent linear model is constructed based on the well-known

geometric rule (secant stiffness to the maximum deformation and the equivalence of dissipation energy).

At first only the bare frame is considered. Let k_0^b, μ^b, ω_{eq} denote the initial stiffness, ductility factor and equivalent natural circular frequency, respectively, of the building structure. The corresponding equivalent stiffness k_{eq}^b and viscous damping coefficient C_{eq}^b of the SDOF model (bare frame) may be described as

(a) $\delta_{max} \leq \delta_y^b$

$$k_{eq}^b = k_0^b \tag{2a}$$

$$C_{eq} = C_0 = 2 \times 0.02 \frac{k_0^b}{\omega} \tag{2b}$$

(b) $\delta_y^b < \delta_{max}$

$$k_{eq}^b = k_0^b / \mu^b \tag{3a}$$

$$C_{eq} = C_{eq}^b + C_0 = \frac{4}{\pi} \frac{k_0^b}{\omega_{eq}\mu^b}\left(1 - \frac{1}{\mu^b}\right) + 2 \times 0.02 \frac{k_0^b}{\omega} \tag{3b}$$

The first term in Eq. 3(b) can be derived from the equivalence of dissipation energy $\pi C_{eq}\omega_{eq}(\mu^b\delta_y^b)^2$ = $4k_0^b\delta_y^b(\mu^b\delta_y^b - \delta_y^b)$.

When a hysteretic damper obeying an elastic-perfectly plastic rule is used in this building structure modeled as an SDOF model, the total force-deformation relation obeys the normal trilinear hysteretic rule. As in the above bare frame case, the equivalent linear model is constructed based on the well-known geometric rule. The corresponding equivalent stiffness k_{eq} and viscous damping coefficient C_{eq} may be described as

(a) $\delta_{max} \leq \delta_y^a$

$$k_{eq} = \frac{(k_0^a + k_0^b) \times \delta_{max}}{\delta_{max}} = k_0^a + k_0^b \tag{4a}$$

$$C_{eq} = C_{eq}^a + C_{eq}^b + C_0 = 0 + 0 + 2 \times 0.02 \frac{k_0^b}{\omega} \tag{4b}$$

(b) $\delta_y^a < \delta_{max} \leq \delta_y^b$

$$k_{eq} = \frac{\left(k_0^a + k_0^b\right) \times \delta_y^a + k_0^b\left(\delta_{max} - \delta_y^a\right)}{\delta_{max}} = \frac{k_0^a \times \delta_y^a + k_0^b \times \delta_{max}}{\delta_{max}} = \frac{k_0^a}{\mu^a} + k_0^b \tag{5a}$$

$$C_{eq} = C_{eq}^a + C_{eq}^b + C_0 = \frac{4}{\pi} \frac{k_0^a}{\omega_{eq}\mu^a}\left(1 - \frac{1}{\mu^a}\right) + 0 + 2 \times 0.02 \frac{k_0^b}{\omega} \tag{5b}$$

(c) $\delta_y^b < \delta_{max}$

$$k_{eq} = \frac{\left(k_0^a + k_0^b\right) \times \delta_y^a + k_0^b(\delta_y^b - \delta_y^a)}{\delta_{max}} = \frac{k_0^a}{\mu^a} + \frac{k_0^b}{\mu^b} \quad (6a)$$

$$C_{eq} = C_{eq}^a + C_{eq}^b + C_0 = \frac{4}{\pi}\frac{k_0^a}{\omega_{eq}\mu^a}\left(1 - \frac{1}{\mu^a}\right) + \frac{4}{\pi}\frac{k_0^b}{\omega_{eq}\mu^b}\left(1 - \frac{1}{\mu^b}\right) + 2 \times 0.02\frac{k_0^b}{\omega} \quad (6b)$$

where δ_{max} is the given maximum deformation of the building structure, δ_y^a is the yield deformation of the hysteretic damper system and δ_y^b is the yield deformation of the building structure. In addition, k_0^a, μ^a, C_{eq}^a are the initial stiffness, ductility factor and viscous damping coefficient, respectively, of the hysteretic damper system.

4.3 Structural model 1 (Elastic frame)

At first an elastic frame model is considered and reduced to an SDOF model. The mass of the model is 2.4×10^4(kg) and the frame stiffness is $k^s = 6.58 \times 10^7$ N/m. The natural period is $T = 0.12$ s. The high-hardness rubber damper (visco-elastic damper, Tani *et al.* 2009) with the thickness $t = 10$ mm and area $S = 1.57 \times 10^5$ mm^2 and three hysteretic dampers with different yield displacements ($\delta_y = 0.5, 1.0, 2.0$ mm) and a common yield strength are used as passive dampers. The initial stiffness of the hysteretic damper is $k^d = 1.32 \times 10^7$ N/m for $\delta_y = 0.5$ mm. Then the common yield strength is obtained as $k^d \times \delta_y = 6.6$ kN.

Fig. 4 shows the restoring-force characteristics of the high-hardness rubber damper and three hysteretic dampers ($\delta_y = 0.5, 1.0, 2.0$ mm). While the high-hardness rubber damper exhibits rather complicated hysteretic restoring-force characteristic (Tani *et al.* 2009), a simplified equivalent linear model has been introduced (Appendix A). On the other hand, an elastic-perfectly plastic restoring-force characteristic is adopted for the hysteretic dampers.

Fig. 5 illustrates the plot of the maximum acceleration of ground motion with respect to the maximum response deformation of the SDOF model which is derived from
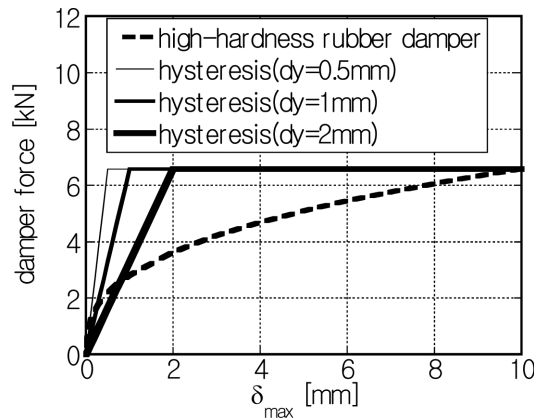

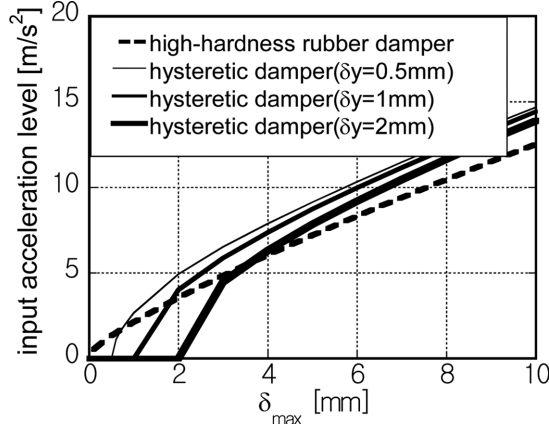Fig. 4 Restoring-force characteristics of high-hardness rubber damper and hysteretic damper

Fig. 5 Maximum acceleration of ground motion with respect to maximum response deformation of SDOF model
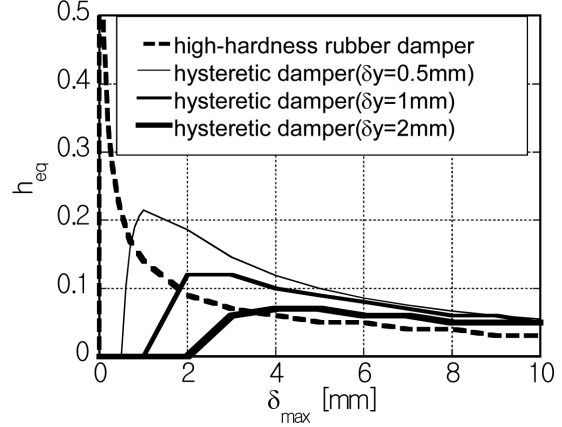
Fig. 6 Equivalent damping ratios with respect to maximum response deformation of SDOF model

$$\ddot{u}_{g\,\text{max}} = a_{\text{max}} = \frac{\omega_{eq}^2 \delta_{\text{max}}}{A_A(h_{eq})} \tag{7}$$

This equation can be obtained from Eq. 1(a) and h_{eq} denotes the equivalent damping ratio. Eq. (7) may be almost equivalent to the relation of the equivalent-performance response acceleration with the maximum deformation by Hayashi (2002) and Hayashi *et al.* (2008). From these plots, the structural designers and engineers can find the maximum response deformation corresponding to the specified input level, e.g. $a_{\text{max}} = 5.0$ m/s^2 for large earthquakes.

When ω becomes smaller than ω_U in Eq. (1), the parameter controlling the input level of ground motion has to be changed from a_{max} to v_{max} and the following relation is derived from Eq. 1(b).

$$\dot{u}_{g\,\text{max}} = v_{\text{max}} = \frac{\omega_{eq}\delta_{\text{max}}}{A_V(h_{eq})} \tag{8}$$

Fig. 6 presents the equivalent damping ratios with respect to the maximum response deformation of the SDOF model. It can be understood from this figure that there exists the optimal deformation attaining the maximum equivalent damping ratio in hysteretic dampers (Inoue ad Kuwahara, 1998).

4.4 Structural model 2 (Inelastic frame)

Building structures usually exhibit inelastic response to large earthquake ground motions. In the following section, an inelastic low-rise steel building structure is considered which is modeled into an SDOF model. Consider two models whose natural periods are $T = 0.2$ s and 0.4 s. The mass of the model is $m = 1.0 \times 10^4$ kg. The structural damping ratio is 0.02. A hysteretic damper ($\delta_y = 2.0$ mm) is used as passive dampers. This yield displacement of the damper reflects the effect of supporting member stiffness. The elastic stiffness of the hysteretic damper is assumed to be the same as that of the frame. As a result, the elastic stiffness of the hysteretic damper installed in the

frame ($T = 0.4$ s) is one-fourth of that installed in the frame ($T = 0.2$ s).

4.5 Implementation of ductility inverse-mapping method in inelastic steel structure

In order to explain the flow of the proposed ductility inverse-mapping method, inelastic steel structures with and without hysteretic dampers are taken as examples.

Fig. 7 shows the relation of the maximum acceleration of ground motion with the maximum deformation and the plot of the spectral acceleration with respect to the maximum deformation for two SDOF models ($T = 0.2$ s, 0.4 s) of inelastic steel structures with and without hysteretic dampers. Fig. 7(a) indicates that relation for steel structures with hysteretic dampers and Fig. 7(b) shows that relation for steel structures without hysteretic dampers. The maximum acceleration of ground motion is specified here as 5(m/s^2). It can be understood that the response reduction can be achieved in SDOF models with hysteretic dampers. Furthermore the property of the maximum deformation with respect to various input levels of ground motion (for example 2.5 m/s^2, 7.5 m/s^2, 10 m/s^2) can be understood directly from this figure. In order to investigate such property by the conventional capacity spectrum method, iterations are usually required. Furthermore the existence of the solution may be uncertain depending on the property of capacity spectra. The step-by-step procedure of the proposed ductility inverse-mapping method is shown in Fig. 2.

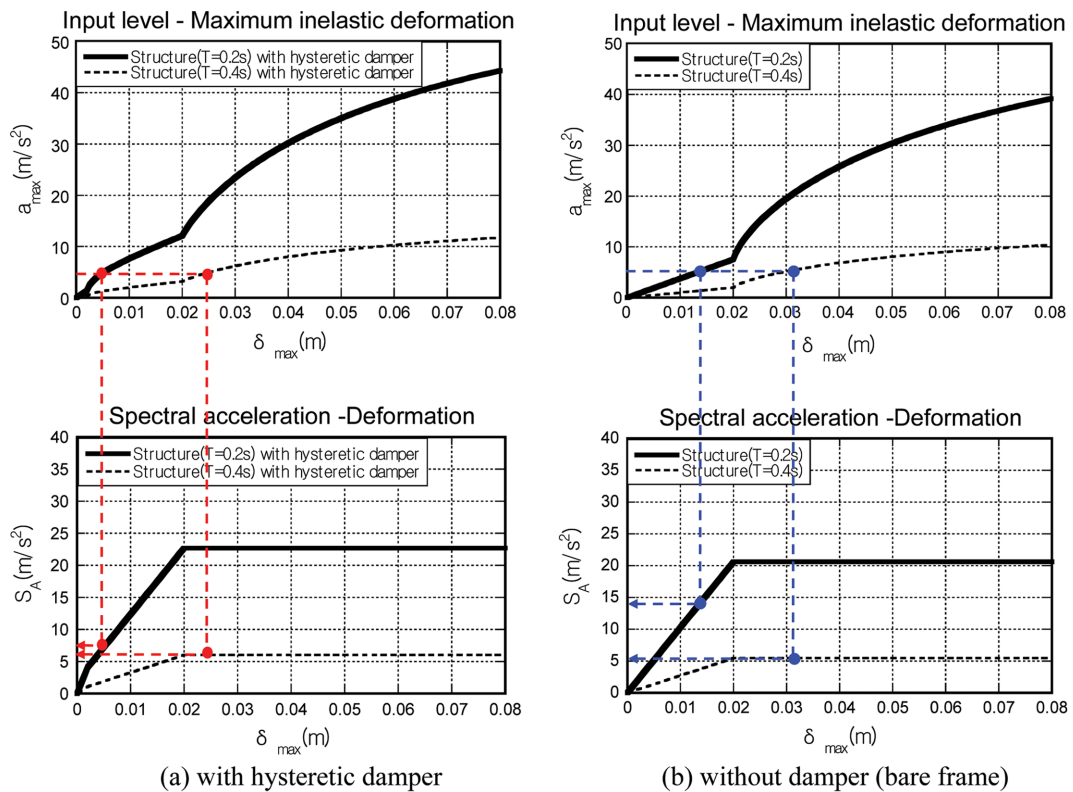(a) with hysteretic damper   (b) without damper (bare frame)

Fig. 7 Relation of maximum acceleration of ground motion with maximum deformation and plot of spectral acceleration with respect to maximum deformation for two SDOF models ($T = 0.2$ s, 0.4 s) with and without hysteretic dampers
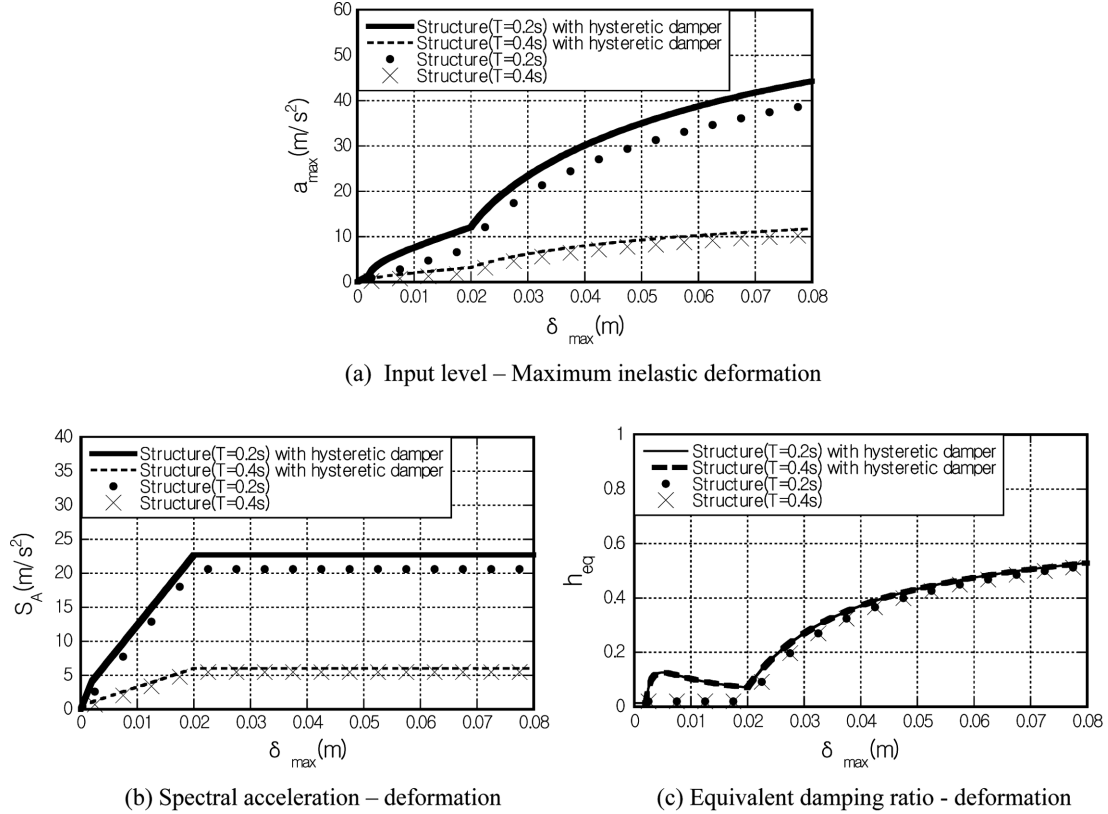
(a) Input level – Maximum inelastic deformation

(b) Spectral acceleration – deformation

(c) Equivalent damping ratio - deformation

Fig. 8 Comparison for two SDOF models (T = 0.2 s, 0.4 s) with and without hysteretic dampers, (a) relation of maximum acceleration of ground motion with maximum deformation, (b) comparison of relation of spectral acceleration with respect to maximum deformation and (c) equivalent damping ratio for maximum deformation

Figs. 8(a) and 8(b) illustrate the comparison of the relation of the maximum acceleration of ground motion with the maximum deformation and the relation of the spectral acceleration with respect to the maximum deformation for two SDOF models (T = 0.2 s, 0.4 s). The corresponding relations with hysteretic dampers are drawn in the same figure. Fig. 8(c) shows the equivalent damping ratio for the maximum deformation. It can be understood from this figure that there exists the sub-optimal deformation (rather smaller deformation range before frame yielding) attaining the local maximum equivalent damping ratio in hysteretic dampers (Inoue and Kuwahara 1998).

Figs. 9(a) and 9(b) present the figures, similar to Figs. 8(a) and 8(b), for two SDOF models (T = 0.2 s, 0.4 s) with and without viscous dampers. Fig. 9(c) shows the equivalent damping ratios for the maximum deformation for viscous dampers and hysteretic dampers. It can be observed that, while the hysteretic dampers are effective in a smaller deformation range (smaller than 0.02 m), the viscous dampers are effective in a larger deformation range.

Fig. 10 shows the conceptual diagram of the relation of the maximum acceleration and velocity of ground motion with the spectral deformation by the proposed method. The design displacement response spectrum by Newmark and Hall (1982) is also plotted in Fig. 10. It can be understood that the parameter controlling the input level of ground motion has to be changed from a_{max} to v_{max}

(a) Input level – Maximum inelastic deformation

(b) Spectral acceleration – deformation
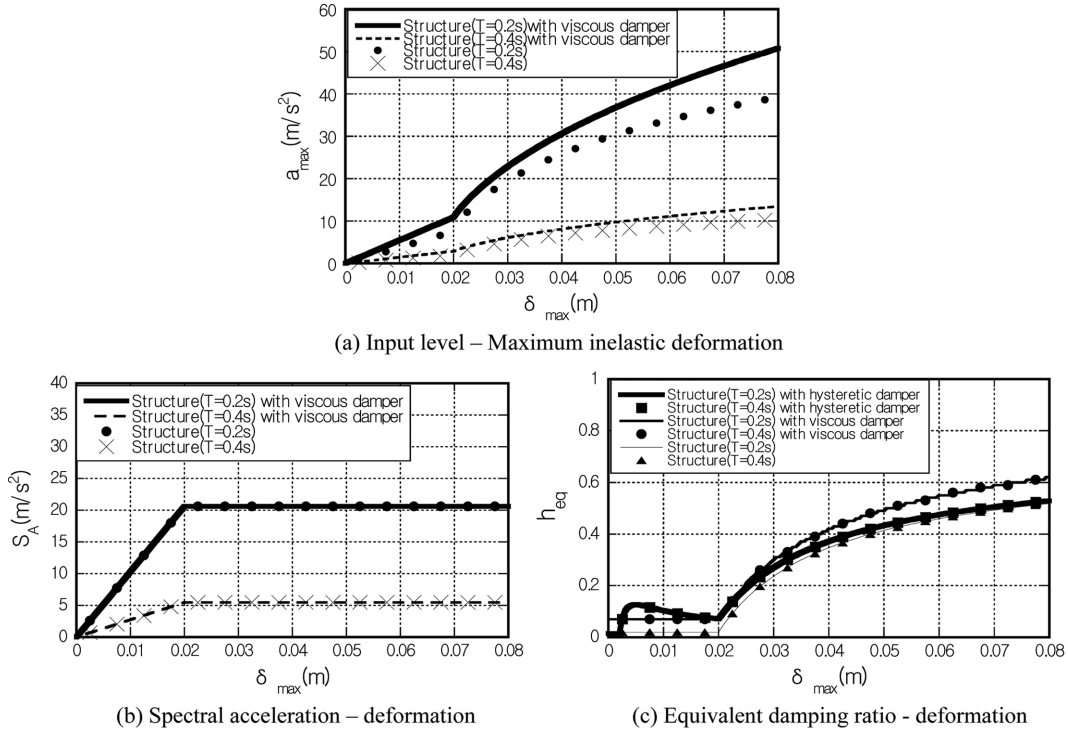

(c) Equivalent damping ratio - deformation

Fig. 9 Comparison for two SDOF models (T = 0.2 s, 0.4 s) with and without viscous dampers, (a) relation of maximum acceleration of ground motion with maximum deformation, (b) comparison of relation of spectral acceleration with respect to maximum deformation and (c) equivalent damping ratio for maximum deformation

$$a_{max} = \frac{\omega_{eq}^2 \delta_{max}}{A_A(h_{eq})}$$

$$v_{max} = \frac{\omega_{eq} \delta_{max}}{A_V(h_{eq})}$$

Input level – Maximum inelastic deformation

Design displacement response spectrum by Newmark and Hall (1982)
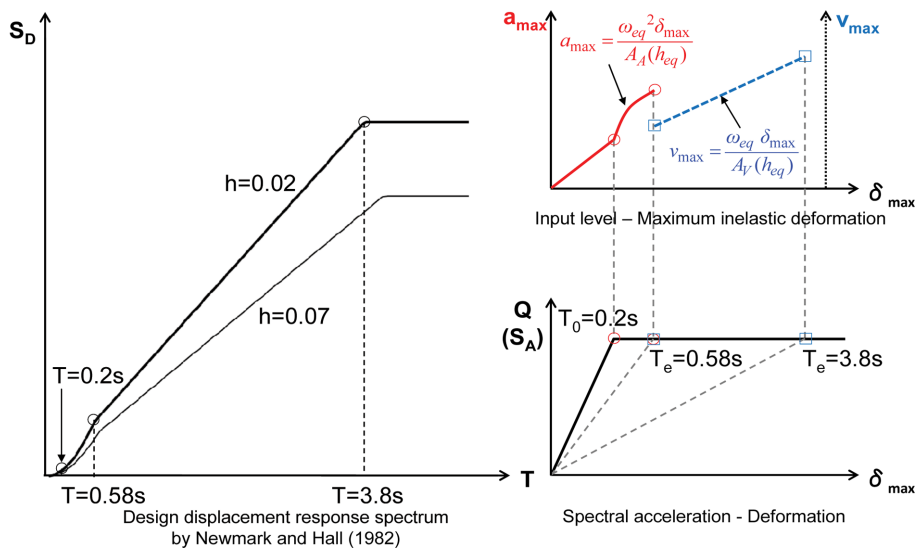
Spectral acceleration - Deformation

Fig. 10 Conceptual diagram of relation of maximum acceleration and velocity of ground motion with spectral deformation (equivalent natural period of SDOF model) by ductility inverse-mapping method and design displacement response spectrum by Newmark and Hall
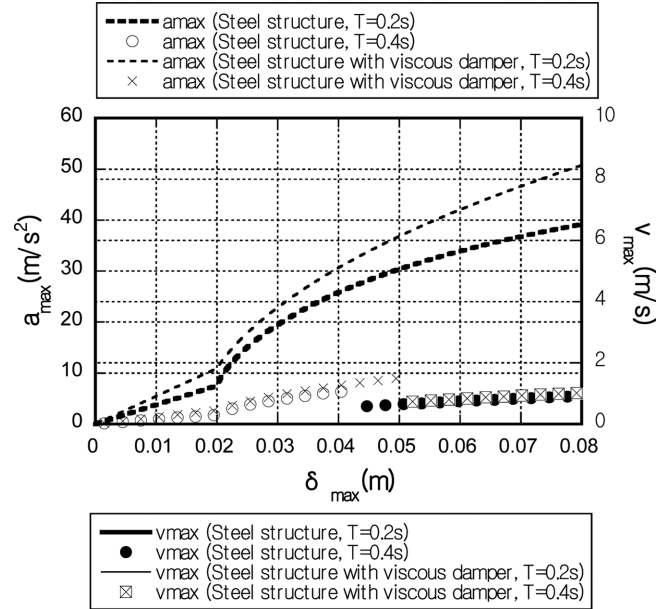
Fig. 11 Relation of maximum acceleration and velocity of ground motion with spectral deformation for two SDOF models (T = 0.2 s, 0.4 s) with and without viscous damper by ductility inverse-mapping method

through the relation of Eq. 1(a) and 1(b). For example, the boundary natural period is 0.58 second in case of considering the structural damping ratio of 0.02.

Fig. 11 presents the relation of the maximum acceleration and velocity of ground motion with the spectral deformation for two SDOF models (T = 0.2 s, 0.4 s) with and without viscous damper obtained by the proposed method. It can be understood that it is necessary to express the input level by the maximum velocity of ground motion as well as by the maximum acceleration for the SDOF model whose natural period is 0.4 second. On the other hand, the equivalent natural period of the SDOF model whose natural period is 0.2 second does not arrive at 0.58 second corresponding to the first inflection point under the range of given maximum deformation. Furthermore, it can be observed that the maximum deformations of the SDOF models with viscous damper at which a_{max} is changed to v_{max} are increased compared with the SDOF models without viscous damper.

4.6 Reinforced concrete, steel and wood structures with various dampers (viscous, visco-elastic and hysteretic dampers)

The proposed ductility inverse-mapping method is applied to reinforced concrete, steel and wood structures to investigate the effectiveness of various passive dampers in various types of building structures. The pros and cons of respective passive dampers are shown in Table 1.

Fig. 12 shows the restoring-force characteristics for two classes of building structures (stiff and flexible) including reinforced concrete, steel and wood structures. The yield story drifts of the reinforced concrete, steel and wood structures have been given by 1/250, 1/125, 1/50. Two steel structures modeled into SDOF models are the same as those treated in Section 4.5 (the natural periods are T = 0.2 s and 0.4 s). In the present theory, the yield deformation and strength are required. Only the information is meaningful that the yield deformation of wood structures is the

Table 1 Pros and cons of passive dampers

	Pros	Cons
Viscous damper	Avoidance of excessive additional force in structural frame (Phase delay and relief mechanism)	Difficulty in responding to impulsive loading
General visco-elastic damper	Cost effective	Introduction of excessive additional force in structural frame Temperature, frequency, amplitude-dependence
High-hardness rubber damper	Low temperature and frequency-dependence, Large initial stiffness and large deformation capacity	Introduction of excessive additional force in structural frame
Hysteretic damper (shear, buckling-restrained brace)	Cost effective	Introduction of excessive additional force in structural frame

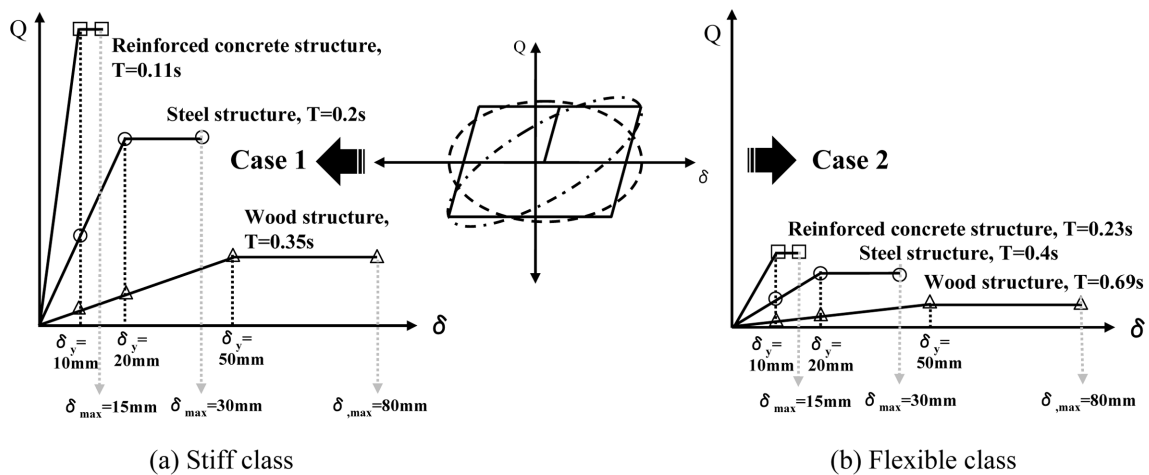(a) Stiff class (b) Flexible class

Fig. 12 Restoring-force characteristics for two classes of building structures (stiff and flexible-type reinforced concrete, steel and wood structures)

largest, that of steel structures is the second and that of reinforced concrete structures is the smallest. The adopted force-deformation relation is one example and has been modeled based on accumulated database (Seismic resistant design manual committee for wood buildings (2004), Tsuji *et al*. (2010)). It is possible to employ more detailed multi-linear force-deformation relations if desired. The proposed ductility inverse-mapping method can be applied to such models without difficulty.

The mass of the model is $m = 1.0 \times 10^4$ kg. The structural damping ratio is 0.02. The natural periods of the reinforced and wood structures without dampers have been determined based on the comparison with those of steel structures and are shown in Fig. 12 together with those of steel structures. The quantities of hysteretic dampers are determined so that the elastic stiffness of the hysteretic damper is assumed to be the same as that of the bare frame for all the cases of reinforced concrete, steel and wood structures. Therefore six hysteretic dampers with different stiffnesses exist. The yield displacement $\delta_y = 2.0$ mm of hysteretic dampers reflects the effect of supporting member

stiffness. On the other hand, the quantities of viscous dampers are specified so that the additional stiffness-proportional damping ratio becomes 0.05 for the model of $T = 0.2$ s and 0.025 for the model of $T = 0.4$ s. As a result, the damping coefficients of viscous dampers are proportional to the stiffnesses of frames with $2 h/\omega$ as the coefficient (h: 0.05 or 0.025, ω: natural circular frequency of the frame). Furthermore the quantities of the visco-elastic dampers are given so that the equivalent stiffness of the visco-elastic dampers at 100% strain ($\delta = 10.0$ mm) is equivalent to that of the hysteretic damper at $\delta = 10.0$ mm.
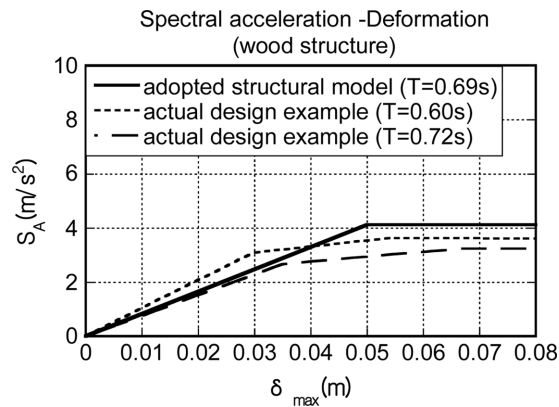

Fig. 13 Validation of restoring-force characteristic of wood structure
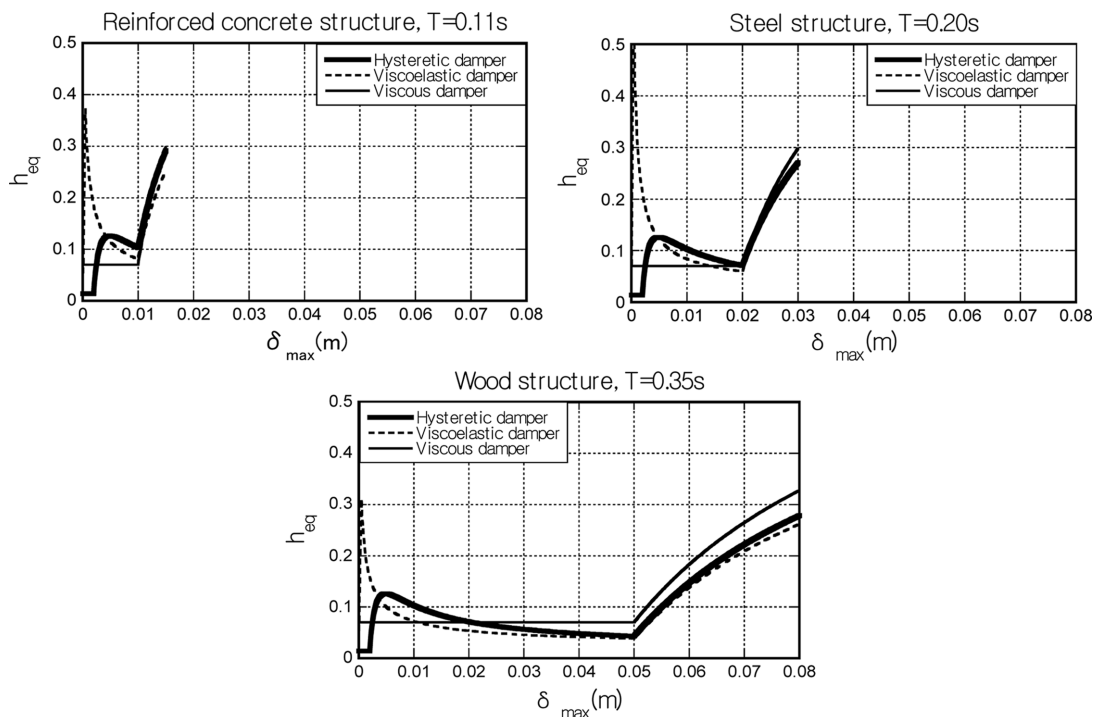

Fig. 14 Equivalent damping ratios with respect to response deformation of reinforced concrete, steel and wood structures with hysteretic, viscous and visco-elastic (high-hardness rubber) dampers (stiff structures)
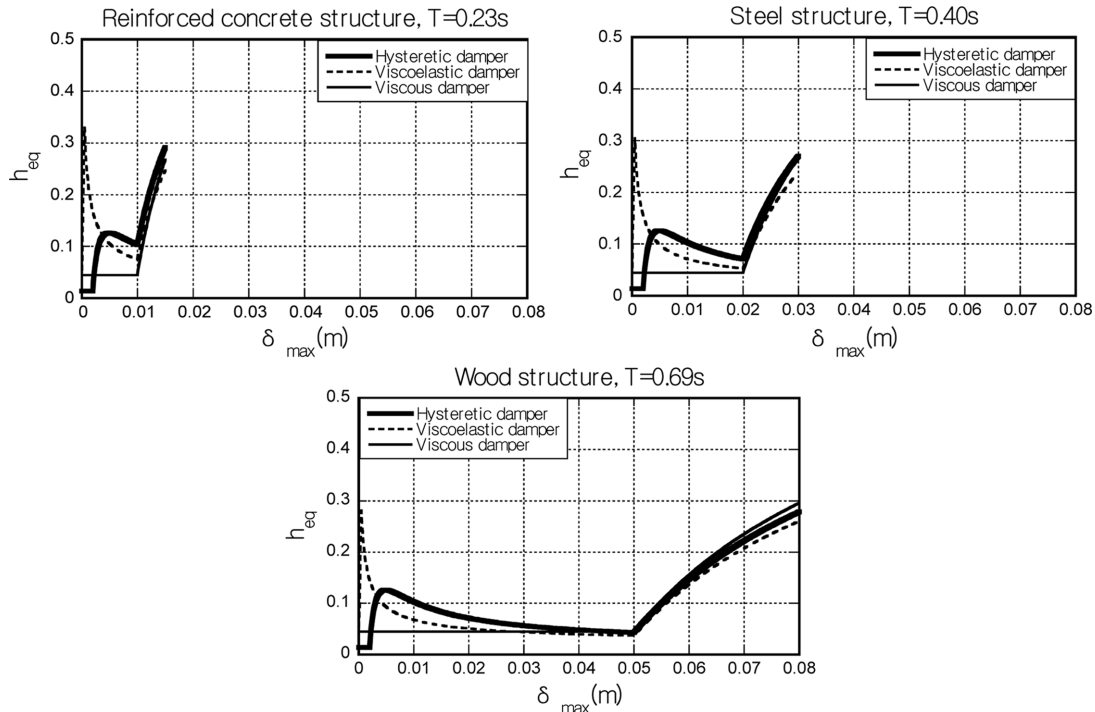
Fig. 15 Equivalent damping ratios with respect to response deformation of reinforced concrete, steel and wood structures with hysteretic, viscous and visco-elastic (high-hardness rubber) dampers (flexible structures)

Fig. 13 shows the validation of the restoring-force characteristic of the wood structure ($T = 0.69$ s). The actual design examples in the figure are taken from the procedure based on the Japanese seismic design code (Seismic resistant design manual committee for wood buildings (2004)). The actual design data have been validated through the comparison with the experimental results. It may be said that the adopted restoring-force characteristic of the wood structure ($T = 0.69$ s) can simulate fairly well the actual ones.

Fig. 14 illustrates the equivalent damping ratios with respect to the response deformation of reinforced concrete, steel and wood structures (stiff structures) with hysteretic, viscous and visco-elastic (high-hardness rubber) dampers. On the other hand, Fig. 15 presents the corresponding figure for flexible structures. It can be observed from Figs. 14 and 15 that, while the visco-elastic and hysteretic dampers are effective in rather small deformation ranges, the viscous dampers are effective in a rather larger deformation range.

4.7 Equivalent linear model (Positive second-branch stiffness)

It is known that the equivalent damping coefficient derived from the geometric rule (Section 4.2) is somewhat larger than the actual value. To respond to this problem, a concept of effective deformation ratio is introduced. This concept is constructed based on the fact that the effective hysteretic energy related to the actual maximum deformation can be described by a reduced energy. In other words, the hysteretic energy derived from the actual deformation is somewhat larger for accurate evaluation of equivalent damping. The reduced energy is assumed to be expressed by the
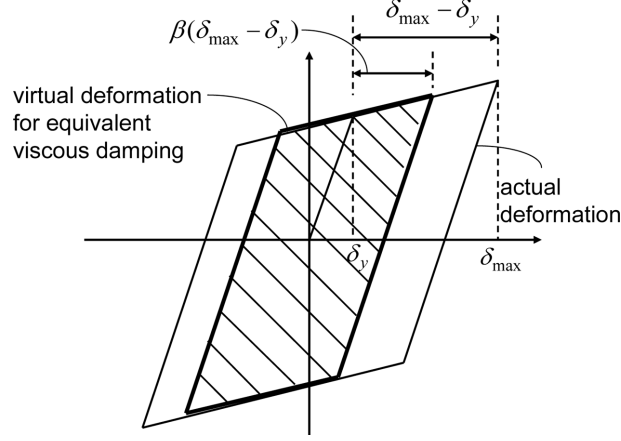
Fig. 16 Effective deformation ratio

effective deformation ratio β multiplied on the maximum plastic deformation to obtain the effective deformation. The conceptual diagram of effective deformation ratio is shown in Fig. 16.

Consider the frame with hysteretic dampers. For the purpose of presenting the fundamental concept of the effective deformation ratio, only the bare frame is considered at first. Let k_0^b and ak_0^b denote the initial stiffness of the bare frame and its second-branch stiffness and let β^b denote the effective deformation ratio. The corresponding equivalent stiffness k_{eq}^b and viscous damping coefficient C_{eq}^b of the SDOF model (bare frame) may be described as

(a) $\delta_{max} \leq \delta_y^b$

$$k_{eq}^b = k_0^b \tag{9a}$$

$$C_{eq} = C_0 = 2 \times 0.02 \frac{k_0^b}{\omega} \tag{9b}$$

(b) $\delta_y^b < \delta_{max}$

$$k_{eq}^b = k_0^b \left\{ \frac{1}{\mu^b} + \alpha \left(1 - \frac{1}{\mu^b} \right) \right\} \tag{10a}$$

$$C_{eq} = C_{eq}^b + C_0 = \frac{4}{\pi} \frac{\beta^b (1-\alpha) k_0^b}{\omega_{eq} \mu^b} \left(1 - \frac{1}{\mu^b} \right) + 2 \times 0.02 \frac{k_0^b}{\omega} \tag{10b}$$

where μ^b and ω_{eq} are the ductility factor and equivalent natural circular frequency of the frame, respectively, as in Section 4.2.

As in the above bare frame case, the equivalent linear model is constructed by using the effective deformation ratio. Let β^a denote the effective deformation ratio of the hysteretic damper. The corresponding equivalent stiffness k_{eq} and viscous damping coefficient C_{eq} may be described as

(a) $\delta_{\max} \leq \delta_y^a$

$$k_{eq} = \frac{(k_0^a + k_0^b) \times \delta_{\max}}{\delta_{\max}} = k_0^a + k_0^b \tag{11a}$$

$$C_{eq} = C_{eq}^a + C_{eq}^b + C_0 = 0 + 0 + 2 \times 0.02 \frac{k_0^b}{\omega} \tag{11b}$$

(b) $\delta_y^a < \delta_{\max} \leq \delta_y^b$

$$k_{eq} = \frac{\left(k_0^a + k_0^b\right) \times \delta_y^a + k_0^b\left(\delta_{\max} - \delta_y^a\right)}{\delta_{\max}} = \frac{k_0^a \times \delta_y^a + k_0^b \times \delta_{\max}}{\delta_{\max}} = \frac{k_0^a}{\mu^a} + k_0^b \tag{12a}$$

$$C_{eq} = C_{eq}^a + C_{eq}^b + C_0 = \frac{4}{\pi} \frac{\beta^a k_0^a}{\omega_{eq} \mu^a}\left(1 - \frac{1}{\mu^a}\right) + 0 + 2 \times 0.02 \frac{k_0^b}{\omega} \tag{12b}$$

(c) $\delta_y^b < \delta_{\max}$

$$k_{eq} = \frac{\left(k_0^a + k_0^b\right) \times \delta_y^a + k_0^b(\delta_y^b - \delta_y^a) + \alpha k_0^b(\delta_{\max} - \delta_y^b)}{\delta_{\max}} = \frac{k_0^a}{\mu^a} + k_0^b\left\{\frac{1}{\mu^b} + \alpha\left(1 - \frac{1}{\mu^b}\right)\right\} \tag{13a}$$

$$C_{eq} = C_{eq}^a + C_{eq}^b + C_0 = \frac{4}{\pi} \frac{\beta^a k_0^a}{\omega_{eq} \mu^a}\left(1 - \frac{1}{\mu^a}\right) + \frac{4}{\pi} \frac{\beta^b(1-\alpha)k_0^b}{\omega_{eq} \mu^b}\left(1 - \frac{1}{\mu^b}\right) + 2 \times 0.02 \frac{k_0^b}{\omega} \tag{13b}$$

where $\delta_{\max}$ is the given maximum deformation of the building structure, δ_y^a is the yield deformation of the hysteretic damper system and δ_y^b is the yield deformation of the building structure as in Section 4.2. In addition, k_0^a, μ^a, C_{eq}^a are the initial stiffness, ductility factor and viscous damping coefficient of the hysteretic damper system, respectively, as in Section 4.2.

4.8 Numerical examples of equivalent linear model for frames with positive second-branch stiffness and viscous dampers

Consider the frame with viscous dampers. In this case, Eqs. 9 and 10 are used. As in Section 4.6, the quantities of viscous dampers are specified so that the additional stiffness-proportional damping ratio becomes 0.05 for the model of $T = 0.2$ s and 0.025 for the model of $T = 0.4$ s. This quantity is added to the structural damping coefficient in Eqs. 9(b) and 10(b).

For accuracy check, the time-history response analysis is conducted in this section. Fig. 17 illustrates the mean response spectrum of five spectrum-compatible ground motions and Fig. 18 presents a sample of acceleration of the spectrum-compatible motion.

Fig. 19 shows the comparison of the relation of the maximum acceleration of ground motion with the maximum deformation for the SDOF model ($T = 0.2$ s) without and with viscous dampers for various effective deformation ratios β^b. The results by the time-history response analysis are also plotted in the same figure. The time-history response analysis has been conducted by using the
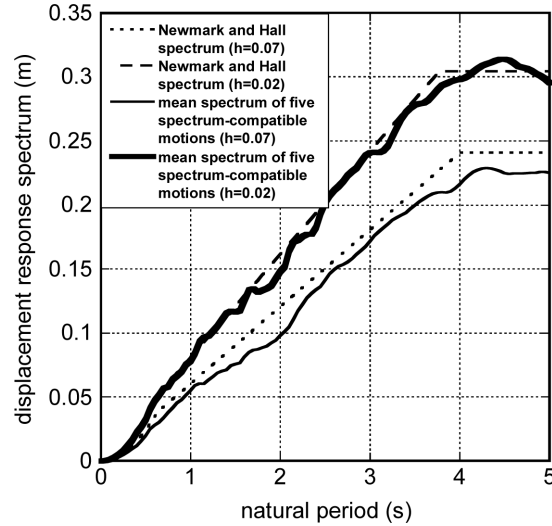
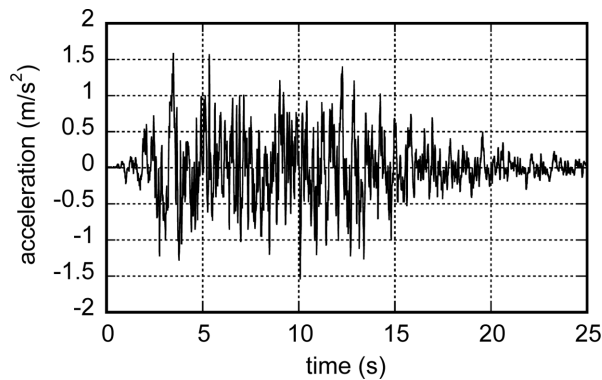Fig. 17 Response spectrum of spectrum-compatible ground motions

Fig. 18 Sample of acceleration of spectrum-compatible motion

Newmark-β method to a set of five spectrum-compatible ground motions generated for several input levels. Fig. 20 illustrates the corresponding figure for the SDOF model ($T = 0.4$ s). It can be observed that, while the effective deformation ratio of 0.1-0.3 is appropriate for the SDOF model of $T = 0.2$ s, that of 0.6 is suitable for the SDOF model of $T = 0.4$ s. The suitable value of effective deformation ratio may be different model by model. The detailed investigation may be necessary in the future. It can also be observed that multiple values of input level (maximum ground acceleration) can exist for the same deformation level. This means that, if the time-history response analysis is used in the conventional capacity spectrum method, the problem of multiple solutions or non-convergence may arise. The proposed ductility inverse-mapping method does not cause these problems.

4.9 Application of effective deformation ratio for structural model 1 (elastic frame)

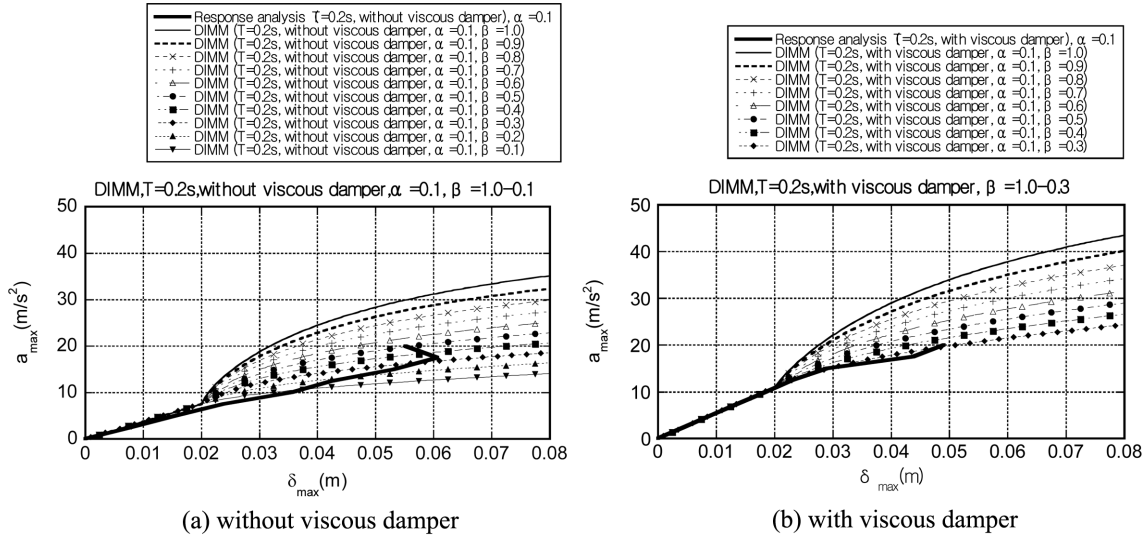Fig. 21 shows the application of the effective deformation ratio of 0.6 for structural model 1

(a) without viscous damper (b) with viscous damper

Fig. 19 Comparison of relation of maximum acceleration of ground motion with maximum deformation for SDOF model ($T = 0.2$ s) without and with viscous dampers for various effective deformation ratios and corresponding result by time-history response analysis
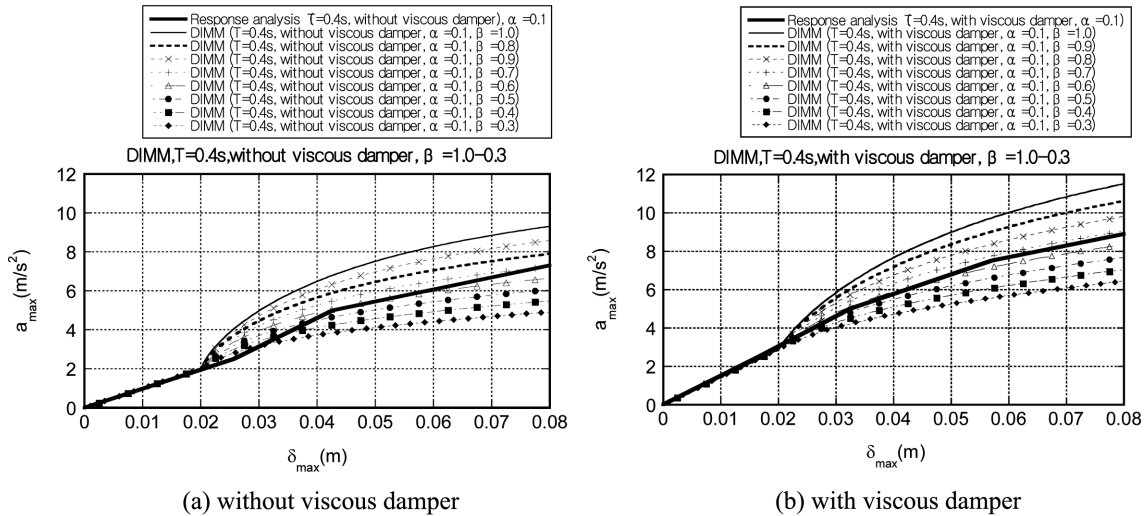

(a) without viscous damper (b) with viscous damper

Fig. 20 Comparison of relation of maximum acceleration of ground motion with maximum deformation for SDOF model ($T = 0.4$ s) without and with viscous dampers for various effective deformation ratios and corresponding result by time-history response analysis

(elastic frame) with hysteretic dampers. The effective deformation ratio is applied to the inelastic deformation of hysteretic dampers. Fig. 21(a) illustrates the maximum acceleration of ground motion with respect to the maximum response deformation of the SDOF model corresponding to Fig. 5. On the other hand, Fig. 21(b) presents the equivalent damping ratios with respect to the maximum response deformation of the SDOF model corresponding to Fig. 6. Furthermore Fig. 22 shows the application of the effective deformation ratio of 0.3 for structural model 1 (elastic frame)
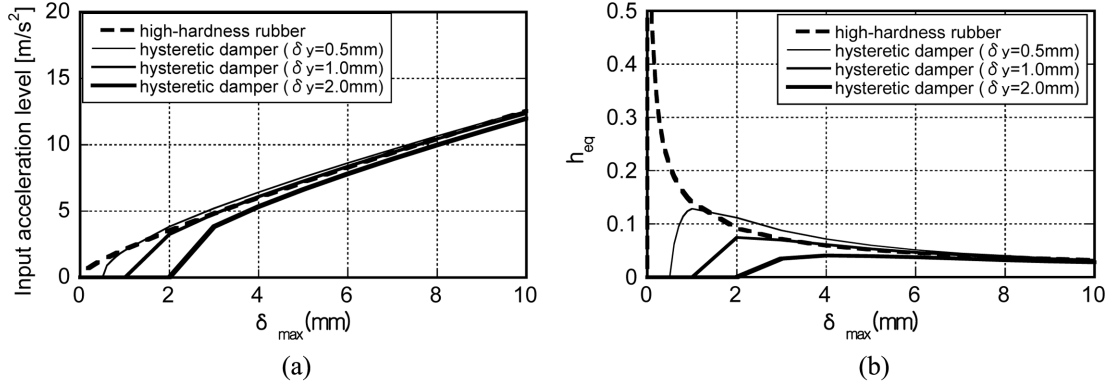
Fig. 21 Application of effective deformation ratio of 0.6 for structural model 1 (elastic frame) with hysteretic dampers, (a) Maximum acceleration of ground motion with respect to maximum response deformation of SDOF model, (b) Equivalent damping ratios with respect to maximum response deformation of SDOF model
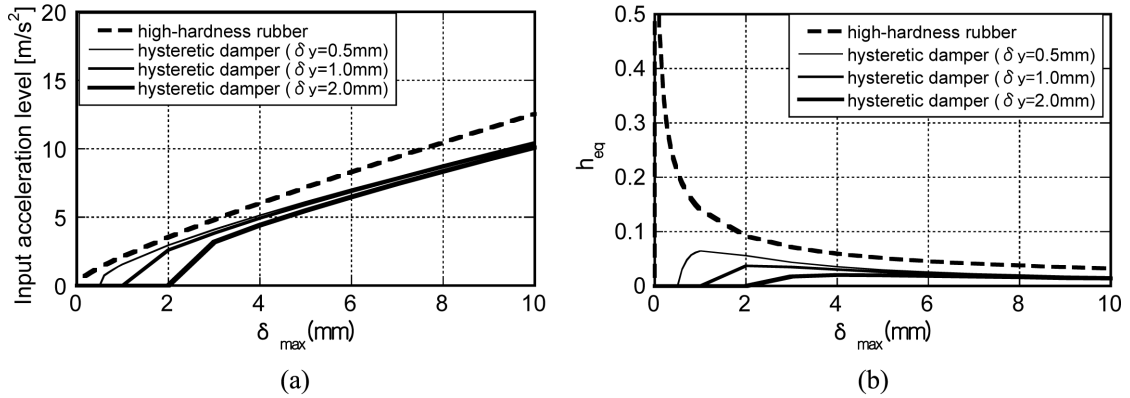

Fig. 22 Application of effective deformation ratio of 0.3 for structural model 1 (elastic frame) with hysteretic dampers, (a) Maximum acceleration of ground motion with respect to maximum response deformation of SDOF model, (b) Equivalent damping ratios with respect to maximum response deformation of SDOF model

with hysteretic dampers. It can be observed that, as the effective deformation ratio becomes smaller, the maximum acceleration of ground motion and the equivalent damping ratio become smaller.

4.10 Limitations of the proposed method

The limitations of the proposed method may be summarized as follows:
(1) The building structures are limited to low-rise buildings because the response evaluation based on the first-mode component is used.
(2) Although the direction for next calculations is clear, successive calculation for varied target deformation is required.
(3) Additional calculation for determining effective deformation ratios is necessary.
(4) The proposed method can not deal with building irregularities.

5. Conclusions

A new concept has been introduced to investigate a preferable passive damper system for the retrofit of various types of houses. The principal results may be summarized as follows.

(1) A ductility inverse-mapping method can be developed via a dynamic pushover analysis which enables one to find the maximum acceleration of ground motion for the prescribed maximum response deformation. In the conventional capacity spectrum method, the maximum response deformation is computed through iterative procedures for the prescribed maximum acceleration of ground motion. While successive calculations are needed, no numerically unstable iterative procedure is required in the proposed method.

(2) The ductility inverse-mapping method has been applied successfully to an SDOF model of bilinear hysteresis. The SDOF models without and with passive dampers (viscous, visco-elastic and hysteretic dampers) have been taken into account to investigate the effectiveness of passive dampers for seismic retrofitting of various types of structures. Since the maximum response deformation is the principal parameter and specified sequentially, the proposed ductility inverse-mapping method is suitable for the implementation of the performance-based design.

(3) There exists the sub-optimal deformation (rather smaller deformation range before frame yielding) attaining the local maximum equivalent damping ratio in SDOF models with hysteretic dampers. It can further be observed that, while the hysteretic dampers are effective in a smaller deformation range, the viscous dampers are effective in a rather larger deformation range.

(4) The concept of effective deformation ratio is very useful and reliable for estimating the maximum inelastic deformation. However further investigation is needed for the evaluation of the appropriate value of effective deformation ratios.

Acknowledgements

References

ATC (1996), *Seismic evaluation and retrofit of concrete buildings*, Vol.1, ATC-40, Applied Technology Council, Redwood City.
BSSC (1997), *NEHRP guidelines for the seismic rehabilitation of buildings*, FEMA-273, developed by ATC for FEMA, Washington, D.C.
Chopra, A.K., Goel, R.K. and Chintanapakdee, C. (2004), "Evaluation of a modified MPA procedure assuming higher modes as elastic to estimate seismic demands", *Earthq. Spectra*, **20**(3), 757-778.
Fajfar, P. (1999), "Capacity spectrum method based on inelastic demand spectra", *Earthq. Eng. Struct. Dyn.*, **28**(9), 979-993.
Freeman, S.A., Nicoletti, J.P. and Tyrell, J.V. (1975), "Evaluations of existing buildings for seismic risk: a case

study of Puget Sound Naval Shipyard, Bremerton, Washington", *Proc. 1st US. National Conf. Earthq. Eng.*, EERI, Berkeley, 113-122.

Freeman, S.A. (1998), "Development and use of capacity spectrum method", *Proc. 6th US. National Conf. Earthq. Eng.*, Seattle, CD-ROM, EERI, Oakland.

Gencturk B. and Elnashai, A.S. (2008), "Development and application of an advanced capacity spectrum method", *Eng. Struct.* **30**(11), 3345-3354.

Guyader, A.C. and Iwan, W.D. (2006), "Determining equivalent linear parameters for use in a capacity spectrum method of analysis", *J. Struct. Eng. - ASCE.*, **132**(1), 59-67.

Hayashi, Y. (2002), "Evaluation of seismic design load based on equivalent-performance response spectra", *Proc. of the 11th Japan Earthquake Engineering Symposium*, 651-656. (in Japanese)

Hayashi, Y., Nii, A. and Morii, T. (2008), "Evaluation of building damage based on equivalent-performance response spectra", *Proc. of the 14th World Conference on Earthquake Engineering*, China.

Inoue, K. and Kuwahara, S. (1998), "Optimum strength ratio of hysteretic damper", *Earthq. Eng. Struct. Dyn.*, **27**(6), 577-588.

Kalkan, E. and Kunnath, S.K. (2006), "Adaptive modal combination procedure for nonlinear static analysis of building structures", *J. Struct. Eng. - ASCE.*, **132**(11), 1721-1731.

Lin, Y.Y. and Miranda, E. (2004), "Non-iterative capacity spectrum method based on equivalent linearization for estimating inelastic deformation demands of buildings", *J. Struct. Mech. Earthq. Eng. - JSCE*, 733(I-69), 113-119.

Newmark, N.M. and Hall, W.J. (1982), "*Earthquake spectra and design*", Earthquake Engineering Research Institute, Berkeley.

Seismic resistant design manual committee for wood buildings (2004), *Seismic resistant design manual for wood buildings*, Gakugei-shuppansya, Kyoto. (in Japanese)

Tani, T., Yoshitomi, S., Tsuji, M. and Takewaki, I. (2009), "High-performance control of wind-induced vibration of high-rise building via innovative high-hardness rubber damper", *J. Struct. Design Tall Special Buildings*, **18**(7), 705-728.

Tsuji, M, Murata, S., Kim, H.G., Yoshitomi, S and Takewaki, I (2010), "Post-tensioning damper system for micro-vibration reduction in residential houses", *J. Struct. Eng. AIJ*, **56B**, 171-178. (in Japanese)

CC

Appendix A: equivalent linear model for high-hardness rubber damper

The high-hardness rubber used in this research has small temperature and frequency dependency compared to general visco-elastic dampers. But it has remarkable strain dependency. The high-hardness rubber shows the equivalent stiffness; $k_{eq\,j}$[N/mm] and damping coefficient $c_{eq\,j}$[Ns/mm] as follows.

$$k_{eq\,j} = \frac{S_j}{d_j}\left(\frac{0.32+0.11\varepsilon^{0.38}}{1+\varepsilon}\,\bar{\gamma}_{\max\,j}^{\;-0.62} + \frac{0.32\varepsilon-0.11\varepsilon^{0.38}}{1+\varepsilon}\,\frac{\bar{\gamma}_{\max\,j}^{\;0.38}}{\gamma_{\max\,j}} + 0.10\gamma_{\max\,j}^{\;-0.66}\right) \quad \text{(A1a)}$$

$$c_{eq\,j} = \frac{S_j}{d_j}\left(\frac{0.64\varepsilon-0.22\varepsilon^{0.38}}{\pi\omega}\,\frac{\bar{\gamma}_{\max\,j}^{\;0.38}}{\gamma_{\max\,j}} + \frac{0.306}{2\pi^2}\left(\frac{\omega}{2\pi}\right)^{-0.75}\gamma_{\max\,j}^{\;-0.75}\right) \quad \text{(A1b)}$$

where

$$\varepsilon = \frac{0.94\left|\gamma_{\max\,j}\right|^{0.73}}{\left|\gamma_{\max\,j}\right|^{0.73}+0.01} \quad \text{(A2)}$$

In Eqs. A1(a), A1(b) for the equivalent linear model for high-hardness rubber dampers, S_j and d_j are the area (mm^2) and the thickness (mm) of the high-hardness rubber damper, $\bar{\gamma}_{\max\,j}$ is the maximum shear strain experienced so far and $\gamma_{\max\,j}$ is the maximum shear strain in the current loop. In this paper $\gamma_{\max\,j} = \bar{\gamma}_{\max\,j}$ is used.